THE JOURNAL OF PHYSICAL CHEMISTRY A

Article

Cite This: J. Phys. Chem. A 2018, 122, 1511−1520

pubs.acs.org/JPCA

Full-Dimensional Quantum Dynamics of SiO in Collision with H_2

Benhui Yang,*[,†] P. Zhang,[‡] Chen Qu,[¶] X. H. Wang,[¶] P. C. Stancil,[†] J. M. Bowman,[¶] N. Balakrishnan,[§] B. M. McLaughlin,[∥] and R. C. Forrey[⊥]

[†]Department of Physics and Astronomy and Center for Simulational Physics, University of Georgia, Athens, Georgia 30602, United States

[‡]Department of Chemistry, Duke University, Durham, North Carolina 27708, United States

[¶]Department of Chemistry, Emory University, Atlanta, Georgia 30322, United States

[§]Department of Chemistry, University of Nevada, Las Vegas, Nevada 89154, United States

[∥]Centre for Theoretical Atomic, Molecular and Optical Physics (CTAMOP), School of Mathematics and Physics, Queen's University Belfast, The David Bates Building, 7 College Park, Belfast BT7 1NN, United Kingdom

[⊥]Department of Physics, Penn State University, Berks Campus, Reading, Pennsylvania 19610, United States

Supporting Information

ABSTRACT: We report the first full-dimensional potential energy surface (PES) and quantum mechanical close-coupling calculations for scattering of SiO due to H_2. The full-dimensional interaction potential surface was computed using the explicitly correlated coupled-cluster (CCSD(T)-F12b) method and fitted using an invariant polynomial approach. Pure rotational quenching cross sections from initial states $v_1 = 0$, $j_1 = 1-5$ of SiO in collision with H_2 are calculated for collision energies between 1.0 and 5000 cm^{-1}. State-to-state rotational rate coefficients are calculated at temperatures between 5 and 1000 K. The rotational rate coefficients of SiO with *para*-H_2 (p-H_2) are compared with previous approximate results which were obtained using SiO-He PESs or scaled from SiO-He rate coefficients. Rovibrational state-to-state and total quenching cross sections and rate coefficients for initially excited SiO ($v_1 = 1$, $j_1 = 0$ and 1) in collisions with p-H_2 ($v_2 = 0$, $j_2 = 0$) and *ortho*-H_2 (o-H_2) ($v_2 = 0$, $j_2 = 1$) are also obtained. The application of the current collisional rate coefficients to astrophysics is briefly discussed.

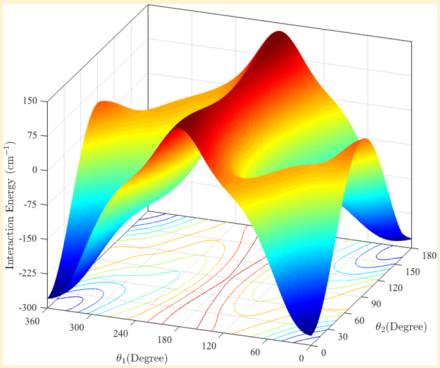

INTRODUCTION

Molecular hydrogen is the most abundant species in most interstellar environments. Collisional relaxation of rotationally or vibrationally excited molecules by H_2 impact is therefore an important process in astrophysics, in astrochemistry, and in many environments where non-equilibrium kinetics plays a dominant role. In the interstellar medium (ISM) cooling processes are primarily associated with collisional thermal energy transfer between internal degrees of freedom followed by emission of radiation. Collisional data for state-to-state vibrational and rotational quenching rate coefficients are needed to accurately model the thermal balance and kinetics in the ISM. Quantum mechanical scattering calculations are the primary source of these much needed collisional data.[1]

A quantum close-coupling (CC) treatment has been developed[2,3] for full-dimensional collisions involving two diatomic molecules. With the continued development of the quantum scattering code TwoBC,[4] which implements full angular momentum coupling, it is now feasible to perform extensive rovibrational coupled-channel scattering calculations for diatom−diatom systems in full dimensionality. The first six-dimensional (6D) CC calculations of rovibrational collisions of H_2 with H_2 were presented recently.[5−7] Subsequently, full-dimensional CC computations were extended to the complex systems CO-H_2[8,9] and CN-H_2[10] on 6D PESs constructed from high-level ab initio electronic structure calculations. However, the full quantum close-coupling method is expensive due to the large number of basis states and coupled channels. Recently this difficulty has been alleviated to some extent by using the coupled-states (CS) approximation presented by Forrey and co-workers.[11,12] The CS approximation has been successfully implemented in H_2 + H_2 and CO + H_2 rovibrational scattering calculations and achieved a reasonable agreement with CC results.[11,12] However, in this work we adopt the CC method.

Interstellar silicon monoxide (SiO) was first detected by Wilson and co-workers[13] through the line emission of $j_1 = 3-2$ in Sgr B2. Recently, Fonfría and co-workers[14] observed SiO transitions ($v_1 = 0, j_1 = 6-5$) and ($v_1 = 1, j_1 = 6-5$) in the ground and first excited vibrational states toward the C-rich AGB star IRC + 10216. However, it was pointed out that fitting the emission of the molecular lines in the warmest regions of the envelopes of AGB stars ($T_k \simeq$ 1000−3000 K) is a

Received: October 2, 2017
Revised: January 22, 2018
Published: January 24, 2018

ACS Publications © 2018 American Chemical Society

DOI: 10.1021/acs.jpca.7b09762
J. Phys. Chem. A 2018, 122, 1511−1520

challenging task due to the lack of collisional coefficients. Tercero and co-workers[15] detected the $j_1 = 2-1$ and $j_1 = 4-3$ lines for the excited $v_1 = 1$ state of SiO in a survey toward Orion KL. Using a radiative transfer code, they modeled the lines of the detected silicon-bearing species. The SiO-H_2 rotational rate coefficients of Dayou and Balança,[16] derived from rigid-rotor approximation calculations on a SiO-He surface, were used in the modeling. Prieto and co-workers[17] detected for the first time toward IK Tau rotational lines of SiO isotopologues in vibrationally excited states. Agúndez and co-workers[18] observed $j_1 = 2-1$ through $j_1 = 8-7$ rotational transitions of the $v_1 = 0$ state and three transitions of the $v_1 = 1$ state of SiO in the inner layers of IRC + 10216. In their radiative transfer modeling, the rate coefficients of Dayou and Balança[16] were adopted for the first 20 rotational levels and for temperatures up to 300 K. However, for temperatures higher than 300 K and for rovibrational transitions, the collision rate coefficients used for carbon monosulfide were adopted. Justtanont and co-workers[19] reported the observation of SiO lines in the Herschel HIFI spectra of nine oxygen-rich AGB stars. These included pure rotational lines ($j_1 = 14-13$ and $j_1 = 16-15$) and vibrationally excited ($v_1 = 1$) rotational lines $j_1 = 13-12$, $j_1 = 15-14$, and $j_1 = 23-22$. Matsuura and co-workers[20] performed nonlocal thermodynamic equilibrium (NLTE) line radiative transfer calculations using the SiO-H_2 collisional excitation rate coefficients which were obtained by scaling the SiO-He values of Dayou and Balança[16] by a factor of 1.38. However, these radiative transfer calculations included only rotational transitions. Ignoring vibrationally excited transitions could potentially cause errors for molecular lines arising from a high-temperature gas, typically over 1000 K. More recently, vibrational excitation calculations of SiO in collision with He have been reported. Using the vibrational close-coupling rotational infinite order sudden method, Balança and Dayou[21] calculated vibrational de-excitation rate coefficients of SiO from the first six vibrational levels.

To the best of our knowledge, no SiO-H_2 PES exists addressing the interaction between SiO and H_2. Pure rotational (de)excitation rate coefficients for some selected rotational levels of SiO with *para*-H_2 (p-H_2) are available, but they were computed using a SiO-He PES and SiO-H_2 reduced mass. Turner and co-workers[22] calculated rotational excitation rate coefficients for SiO in collision with p-H_2 ($j_2 = 0$) using the coupled-states approximation method and a SiO-He PES obtained from an electron gas model.[23] Dayou and Balança[16] constructed a 2D SiO-He potential energy surface based on highly correlated ab initio calculations. This SiO-He PES was also used to compute rate coefficients for the rotational (de)excitation of SiO by collision with p-H_2 ($j_2 = 0$). Even though these SiO-H_2 rate coefficients are approximate and not accurate, they are still used in a variety of astrophysical modeling applications.

Here we present the first full-dimensional PES for the SiO-H_2 complex. We also performed the first scattering calculations for this system for rotational and vibrational inelastic processes in full dimensionality. The paper is organized as follows. The theoretical methods are briefly described in section II. The results are presented and discussed in section III. Astrophysical applications are discussed in section IV. Section V summarizes the results and presents an outlook on future work.

THEORETICAL METHODS

In this section the theoretical methods used in the PES calculation and fit as well as in the rovibrational inelastic scattering calculation are briefly described. The reader is referred to refs 5, 8, and 24 for more details on the methodology.

Potential Energy Surface Computations and Fit. The 6D interaction potential of SiO-H_2 in the electronic ground state was calculated on a 6D grid using Jacobi coordinates (R, r_1, r_2, θ_1, θ_2, ϕ) as shown in Figure 1. The distance between the

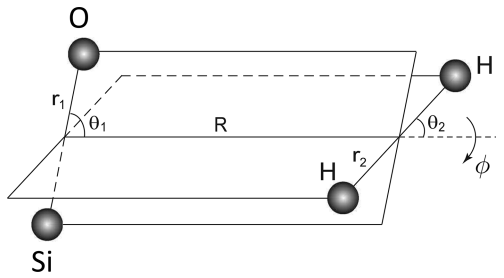

Figure 1. Six-dimensional Jacobi coordinates for the SiO-H_2 system.

centers of mass of SiO and H_2 is denoted by R, while r_1 and r_2 refer to the bond lengths describing the vibration of SiO and H_2, respectively. The angle θ_1 (θ_2) is the in-plane orientation angle between $\vec{r}_1$ ($\vec{r}_2$) and $\vec{R}$, and ϕ the out-of-plane dihedral angle. In the ab initio calculations, the intermolecular distance R was chosen in the range of 4.0−21.0 a_0 and the bond distances are taken over the ranges 2.5 $a_0 \le r_1 \le 3.4$ a_0 and 1.0 $a_0 \le r_2 \le 2.25$ a_0. Here $a_0 = 0.529$ Å is the Bohr radius. The PES was computed with the MOLPRO suite of computational chemistry codes.[25,26] To produce an accurate 6D PES with proper symmetry, the ab initio calculations were performed over the angular coordinates $0° \le \theta_1 \le 360°$, $0° \le \theta_2$ and $\phi \le 180°$, where $\theta_1 = \theta_2 = 0°$ corresponds to the collinear configuration Si−O−H−H.

The ab initio electronic structure computations of potential energies were performed using the explicitly correlated coupled-cluster (CCSD(T)-F12b) method.[27,28] All calculations employed an aug-cc-pVQZ (for H and O atoms)[29] and aug-cc-pwCVQZ (for Si atom) orbital basis set[30] and the corresponding MP2FIT auxiliary bases[31,32] for density fitting. The aug-cc-pV6Z-RI auxiliary bases (without k functions)[33] were used for the resolutions of the identity and density-fitted Fock matrices for all orbital bases. Benchmark calculations at this CCSD(T)-F12 level were carried out on selected molecular configurations, and results were compared with those from the conventional CCSD(T) method using aug-cc-pV5Z. The counter poise (CP)[34] corrected interaction energy agrees closely with those derived from CCSD(T)/aug-cc-pV5Z. The interaction PES was corrected for basis set superposition error (BSSE).[35] No scaled triples correction was used in our calculation.

The 6D SiO-H_2 interaction potential, referred to as VSiOH2, is a hybrid that combines a fit to the full ab initio data set (denoted V_I) and a fit to the long-range data (denoted V_{II}) and is given by

$$V = (1 - s)V_I + sV_{II} \quad (1)$$

where s is a switching function, defined as

DOI: 10.1021/acs.jpca.7b09762
J. Phys. Chem. A 2018, 122, 1511−1520

$$s = \begin{cases} 0 & (R < R_i) \\ 10b^3 - 15b^4 + 6b^5 & (R_i < R < R_f), \\ 1 & (R > R_f) \end{cases} \quad (2)$$

R_i = 10.0 a_0, R_f = 12.0 a_0, and $b = (R-R_i)/(R_f-R_i)$.

Both V_I and V_{II} have been fitted in 6D using an invariant polynomial method[24,36] and are expanded in the form

$$V(y_1 \ldots y_6) = \sum_{n_1 \ldots n_6} C_{n_1 \ldots n_6} y_1^{n_1} y_6^{n_6} (y_2^{n_2} y_3^{n_3} y_4^{n_4} y_5^{n_5} + y_2^{n_3} y_3^{n_2} y_4^{n_5} y_5^{n_4}) \quad (3)$$

where $y_i = \exp(-d_i/p)$ are Morse-type variables and p is a user-specified parameter. For V_I we used p = 3.0 a_0, and for V_{II}, p = 9.5 a_0. The internuclear distances d_i between two atoms are defined as $d_1 = d_{SiO}$, $d_2 = d_{SiH}$, $d_3 = d_{SiH}$, $d_4 = d_{OH}$, $d_5 = d_{OH}$, and $d_6 = d_{HH}$. The powers n_1, ..., n_6 satisfy $n_1 + \ldots + n_6 \leq 7$ and $n_2 + n_3 + n_4 + n_5 \neq 0$, that is, the maximum power of the polynomial is 7, and the interaction potential is guaranteed to go to zero when SiO and H_2 are separated to $R \rightarrow \infty$ for all r_1 and r_2. The total number of linear coefficients $C_{n_1 \ldots n_6}$ is 882, and these coefficients were determined via linear least-squares fitting using our software MSA.[37] The root-mean-square (RMS) fitting error in the long-range fit of V_{II} is 0.05 cm^{-1}, and for V_I the RMS error is 2.61 cm^{-1}. This hybrid approach greatly improves the behavior of the PES in the long range.

Figure 2 shows the R dependence of 6D PES for $(\theta_1, \theta_2, \phi)$ = (0°, 0°, 0°), (180°, 0°, 0°), (180°, 90°, 0°), and (90°, 90°, 90°).

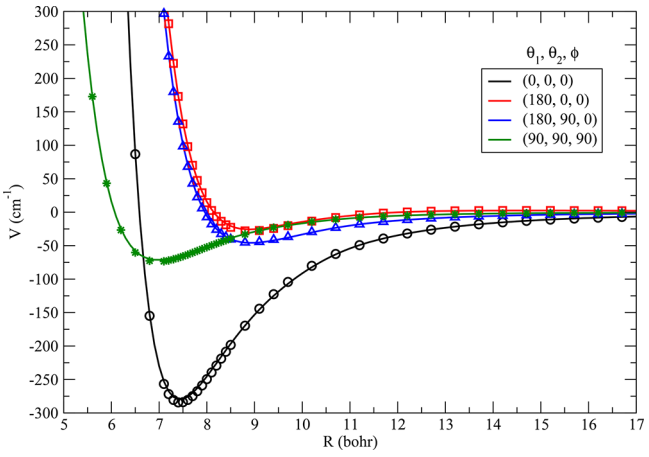

Figure 2. R dependence of the SiO-H_2 PES and VSiOH2 for $(\theta_1, \theta_2, \phi)$ = (0°, 0°, 0°), (180°, 90°, 0°), (90°, 90°, 90°), and (180°, 0°, 0°). The bond lengths of SiO and H_2 are fixed at their equilibrium distances. Symbols are ab initio energy points.

Symbols are energy points from ab initio calculations. The good agreement between ab initio energy points and the fitted PES confirms the accuracy of our fitted PES. In Figure 3 (upper panel) we show a two-dimensional contour plot of the VSiOH2 PES in θ_1, θ_2 space for fixed values of r_1 = 2.8530 a_0, r_2 = 1.4011 a_0, R = 7.5 a_0, and ϕ = 0°. To show the dependence of the PES on r_1 and r_2, a two-dimensional contour plot in r_1, r_2 space for fixed values of R = 7.5 a_0 and $\theta_1 = \theta_2 = \phi$ = 0° is also displayed in the lower panel of Figure 3. The coordinates for the global minimum of −279.5 cm^{-1} for the fitted potential and −284.2 cm^{-1} for the ab initio data correspond to $(R, r_1, r_2, \theta_1, \theta_2, \phi)$ = (7.4 a_0, 2.8530 a_0, 1.4011 a_0, 0°, 0°, 0°).

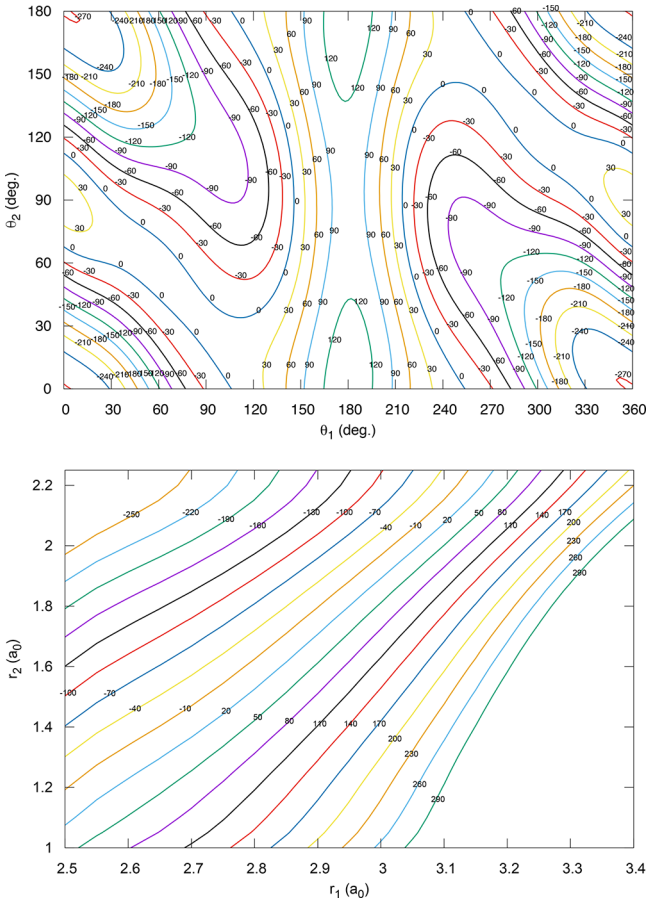

Figure 3. Contour plots of the potential VSiOH2 as a function of θ_1 and θ_2 (upper panel) for r_1 = 2.8530 a_0, r_2 = 1.4011 a_0, R = 7.5 a_0, and ϕ = 0°, and of r_1 and r_2 (lower panel) for R = 6.5 a_0 and $\theta_1 = \theta_2 = \phi$ = 0°. Additional PES plots can be found in the Supporting Information.

Scattering Theory and Computational Details. The quantum CC formalism for diatom−diatom scattering including vibrational motion has been fully developed[2,38−40] and applied to a number of full-dimensional scattering studies.[6,8,10] To facilitate the scattering calculations, the interaction potential between SiO and H_2, $V(\vec{r}_1,\vec{r}_2,\vec{R})$, which vanishes when SiO and H_2 are far apart, can be written as

$$V(R, r_1, r_2, \theta_1, \theta_2, \phi) = \sum_{\lambda_1\lambda_2\lambda_{12}} A_{\lambda_1\lambda_2\lambda_{12}}(r_1, r_2, R) Y_{\lambda_1\lambda_2\lambda_{12}}(\hat{r}_1, \hat{r}_2, \hat{R}) \quad (4)$$

with the bispherical harmonic function expressed as

$$Y_{\lambda_1\lambda_2\lambda_{12}}(\hat{r}_1, \hat{r}_2, \hat{R}) = \sum_{m_{\lambda_1} m_{\lambda_2} m_{\lambda_{12}}} \langle \lambda_1 m_{\lambda_1} \lambda_2 m_{\lambda_2} | \lambda_{12} m_{\lambda_{12}} \rangle \times Y_{\lambda_1 m_{\lambda_1}}(\hat{r}_1) Y_{\lambda_2 m_{\lambda_2}}(\hat{r}_2) Y^*_{\lambda_{12} m_{\lambda_{12}}}(\hat{R}) \quad (5)$$

where $\langle \lambda_1 m_{\lambda 1} \lambda_2 m_{\lambda 2} | \lambda_{12} m_{\lambda 12} \rangle$ is a Clebsch−Gordan coefficient, $0 \leq \lambda_1 \leq 8$, and $0 \leq \lambda_2 \leq 4$. Only even values of λ_2 contribute due to the homonuclear symmetry of H_2.

A combined molecular-state (CMS)[5] notation, $(v_1 j_1 v_2 j_2)$, was applied to describe a combination of rovibrational states for SiO $(v_1 j_1)$ and H_2 $(v_2 j_2)$. The quantum numbers j and v denote the rotational and vibrational energy levels, respectively. The state-to-state rovibrational cross section can be expressed as a function of the collision energy E_c

DOI: 10.1021/acs.jpca.7b09762
J. Phys. Chem. A 2018, 122, 1511−1520

$$\sigma_{v_1j_1v_2j_2\rightarrow v_1'j_1'v_2'j_2'}(E_c) = \frac{\pi}{(2j_1+1)(2j_2+1)k^2} \times \sum_{j_{12}j_{12}'ll'J\varepsilon_l} (2J+1) |\delta_{v_1j_1v_2j_2l,v_1'j_1'v_2'j_2'l'} - S^{J\varepsilon_l}_{v_1j_1v_2j_2l,v_1'j_1'v_2'j_2'l'}(E_c)|^2 \quad (6)$$

where $(v_1j_1v_2j_2)$ and $(v_1'j_1'v_2'j_2')$ denote the initial and final CMSs, respectively. The wave vector $k = \sqrt{2\mu E_c/\hbar^2}$, and S is the scattering matrix. The quantum number l denotes the orbital angular momentum, and the total angular momentum $\vec{J}$ is given by $\vec{J} = \vec{l} + \vec{j}_{12}$, where $\vec{j}_{12} = \vec{j}_1 + \vec{j}_2$.

The total quenching cross section of SiO from initial state $(v_1j_1v_2j_2) \rightarrow (v_1'; v_2'j_2')$ was obtained by summing the state-to-state quenching cross sections over the final rotational state of j_1' of SiO in vibrational state v_1',

$$\sigma_{v_1j_1v_2j_2\rightarrow v_1'; v_2'j_2'}(E_c) = \sum_{j_1'} \sigma_{v_1j_1v_2j_2\rightarrow v_1'j_1'v_2'j_2'}(E_c) \quad (7)$$

The state-to-state rate coefficients at a temperature T can be obtained by thermally averaging the corresponding integral cross sections over a Maxwellian kinetic energy distribution

$$k_{v_1j_1v_2j_2\rightarrow v_1'j_1'v_2'j_2'}(T) = \left(\frac{8}{\pi\mu\beta}\right)^{1/2} \beta^2 \int_0^\infty E_c\sigma_{v_1j_1v_2j_2\rightarrow v_1'j_1'v_2'j_2'}(E_c) \exp(-\beta E_c)\, dE_c \quad (8)$$

where μ is the reduced mass of the SiO-H_2 complex, $\beta = (k_BT)^{-1}$, and k_B is Boltzmann's constant.

Full-dimensional rovibrational scattering calculations were carried out using the TwoBC code[4] in which the CC equations propagated for each value of R from 4 to 21.0 a_0 using the log-derivative matrix propagation method of Johnson.[41] The number of Gauss-Hermite quadrature points N_{r_1}, N_{r_2}; the number of Gauss-Legendre quadrature points in θ_1 and θ_2, N_{θ_1}, N_{θ_2}; and the number of Chebyshev quadrature points in ϕ, N_ϕ adopted to project out the expansion coefficients of the PES are listed in Table 1. For the monomer potentials, we used the results of Barton and co-workers[42] for SiO and Schwenke[43] for H_2.

Table 1. Parameters Used in the Scattering Calculations

	basis set	N_{θ_1} (N_{θ_2})	N_ϕ	N_{r_1} (N_{r_2})	λ_1	λ_2	
			6D Rotation				
p-H_2-SiO	$j_1 = 30, j_2 = 2$	12	8	18	8	4	(16, 30, 80, 230)[b]
o-H_2-SiO	$j_1 = 30, j_2 = 3$	12	8	18	8	4	(18, 32, 82, 232)[b]
			6D Rovibration				
p-H_2-SiO	[(0,35;1,20) (0,2)][a]	12	8	18	8	4	(16, 30, 80, 230)[b]
o-H_2-SiO	[(0,35;1,20) (0,3)][a]	12	8	18	8	4	(18, 32, 82, 232)[b]

[a]Basis set $[(v_1 = 0, j^{max}_{v_1=0}; v_1 = 1, j^{max}_{v_1=1})(v_2 = 0, j^{max}_{v_2=0})]$ is presented by the maximum rotational quantum number $j^{max}_{v_1}$ and $j^{max}_{v_2}$ included in each relevant vibrational level v_1 and v_2 for SiO and H_2, respectively. [b]Maximum partial waves $J(J_{E_1}J_{E_2}J_{E_3}J_{E_4})$ used in scattering calculations for collision energies E_1 = 10, E_2 = 100, E_3 = 1000, and E_4 = 5000 cm^{-1}, respectively.

RESULTS AND DISCUSSION

Pure Rotational Excitation. The rotational excitation and de-excitation cross sections of SiO by H_2 have been calculated for the process, SiO $(v_1 = 0, j_1)$ + H_2 $(v_2 = 0, j_2)$ → SiO $(v_1' = 0, j_1')$ + H_2 $(v_2' = 0, j_2')$. The calculations were carried out in full dimensionality with the VSiOH2 PES and the TwoBC code, with both SiO and H_2 being in their ground vibrational states $v_1 = v_2 = 0$. The initial rotational states of SiO are $j_1 = 0$–5, with the collision energy ranging from 1 to 5000 cm^{-1}. The cross sections with respect to partial wave summation converged to within ~5%, which is ensured by varying the maximum number of partial waves considered (see Table 1). The basis sets used in the scattering calculations are given in Table 1. Figure 4

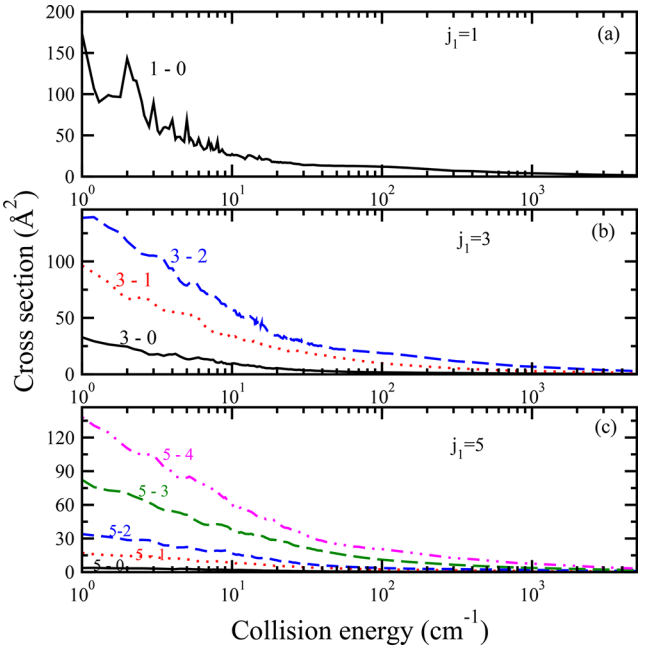

Figure 4. Rotational state-to-state de-excitation cross sections for SiO (j_1) + H_2 $(j_2 = 1)$ → SiO (j_1') + H_2 $(j_2' = 1)$, j_1 = 1, 3, and 5, $j_1' < j_1$.

displays the state-to-state quenching cross section of SiO with p-H_2 $(j_2 = 0)$ from an initial j_1 = 1, 3, and 5. It is seen that for all initial j_1 states, the state-to-state quenching cross sections are dominated by $\Delta j_1 = j_1' - j_1 = -1$ transitions. The cross sections generally increase with increasing j_1' with the smallest cross sections corresponding to transitions to $j_1' = 0$ (largest Δj_1), following a typical exponential energy-gap law behavior. All of the cross sections display some resonances, particularly at collision energies below 20 cm^{-1} due to quasibound states supported by the attractive part of the interaction potential. It is also found that the cross sections are comparable for *ortho*-H_2 (o-H_2) and p-H_2 colliders.[a]

Figure 5(a) and (b) illustrate the total rotational quenching cross section of SiO with p- and o-H_2, respectively. It is seen that except for low collision energies below ~5 cm^{-1}, the total quenching cross sections increase with increasing initial j_1. The resonances present in the state-to-state cross sections can also be observed in the total quenching cross sections.

State-to-state rate coefficients for temperatures between 5 and 1000 K were computed for SiO initial rotational states j_1 = 1–5. As an example, in Figure 6 the state-to-state quenching rate coefficients from initial rotational states j_1 = 1, 3, and 5 are displayed for SiO in collision with p-H_2 $(j_2 = 0)$. Figure 6 shows

DOI: 10.1021/acs.jpca.7b09762
J. Phys. Chem. A 2018, 122, 1511–1520

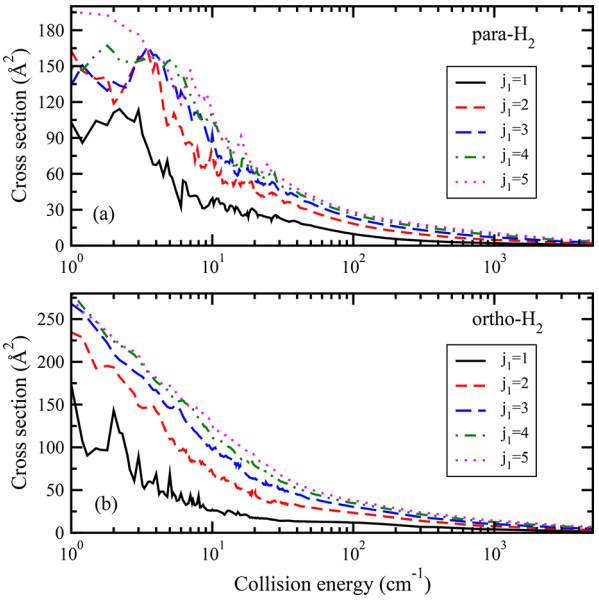

Figure 5. Total rotational de-excitation cross section for SiO from initial rotational states $j_1 = 1-5$ in collisions with (a) p-H_2 ($j_2 = 0$) and (b) o-H_2 ($j_2 = 1$).

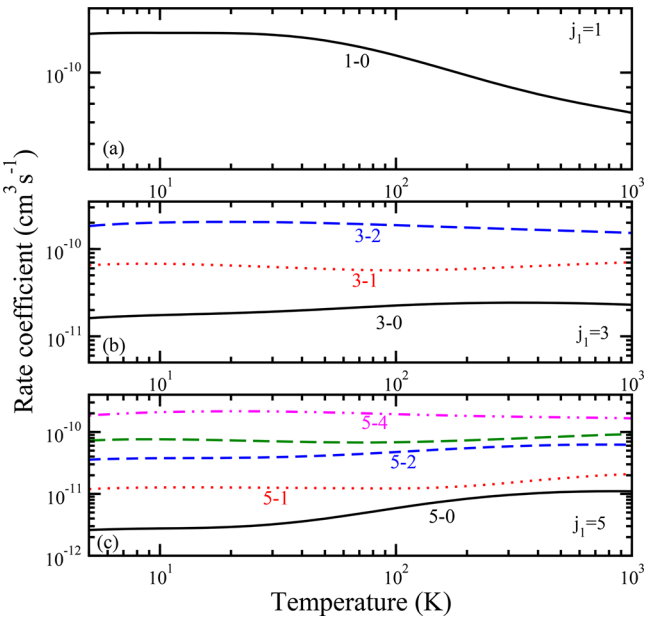

Figure 6. Rotational state-to-state de-excitation rate coefficients for SiO (j_1) + H_2 ($j_2 = 0$) → SiO (j_1') + H_2 ($j_2' = 0$), $j_1 = 1$, 3, and 5, $j_1' < j_1$.

that for both colliders the rate coefficients decrease with increasing $|\Delta j_1| = |j_1' - j_1|$, with $\Delta j_1 = -1$ having the dominant transitions. For all of the selected initial states, the rate coefficients are generally flat except for some undulations due to resonances in the cross sections, mostly for $\Delta j_1 = -1$ transitions.

To the best of our knowledge, there have been no published experimental cross sections or rate coefficients available for rotational transitions of SiO by collisions with H_2. Theoretical studies are also very limited. For SiO in collision with p-H_2 ($j_2 = 0$), pure rotational (de)excitation rate coefficients for some selected rotational levels are available, but they were computed using SiO-He PESs. Turner and co-workers[22] calculated rotational excitation rate coefficients for SiO in collision with p-H_2 ($j = 0$) using the coupled-states approximation and a SiO-He PES obtained from an electron gas model.[23] Dayou and Balança[16] constructed a 2D SiO-He potential energy surface. This SiO-He PES was also used to compute rate coefficients for the rotational (de)excitation of SiO by collision with p-H_2 ($j_2 = 0$). Due to the assumed similarity of p-H_2 and He, the rate coefficient of SiO-p-H_2 ($j_2 = 0$) may also be estimated from the corresponding results for collision with He using the reduced mass scaling factor of 1.4.[44] As examples, we compare in Figures 7 and 8 our accurate rotational rate coefficients with the

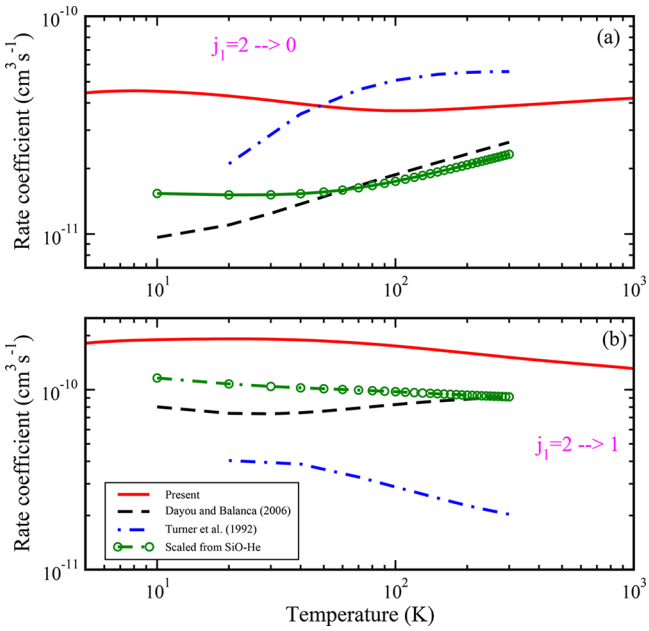

Figure 7. Comparison of current state-to-state rotational quenching rate coefficients with previous approximate results from refs 16 and 22 and obtained from reduced mass scaling of SiO. Transitions are from $j_1 = 2$ to $j_1' = 0$ and 1, and the collider is p-H_2.

approximate SiO-H_2 rate coefficients obtained using SiO-He PESs[16,22] and mass scaling. One can see that there are significant differences between the current state-to-state rate coefficients and the approximate results. Our results are generally larger than the approximate ones, except for the de-excitation transitions $j_1 = 2 \rightarrow 0$, $4 \rightarrow 0$, and $4 \rightarrow 2$ of Turner and co-workers, which become largest at temperatures above ~60 K. It is also worth noting that the global minimum of the 2D SiO-He PES of Dayou and Balança[16] is −26.596 cm^{-1} which is much shallower than the global well depth of VSiOH2 PES. Therefore, the large discrepancies indicate that the use of an SiO-He PES or the simple mass scaling method is not suitable to estimate the rate coefficients of SiO with p-H_2, while a more accurate scaling method may be adopted.[45]

Rovibrational Quenching. The main focus of this work is actually on full-dimensional calculations of the state-to-state cross sections for SiO rovibrational transitions from $v_1 = 1$, SiO ($v_1 = 1$, j_1) + H_2 ($v_2 = 0$, j_2) → SiO ($v_1' = 0$, j_1') + H_2 ($v_2' = 0$, j_2'). For collision energies ranging from 1 to 5000 cm^{-1}, the basis sets used in the scattering calculations are listed in Table 1. The state-to-state cross sections are summed over SiO final rotational levels $v_1' = 0$, j_1' to yield total vibrational quenching cross sections. In the present calculations, $j_1 = 0$ and 1, $j_1' = 0$, 1, 2, ..., 35. Additionally, $j_2 = 0$ for p-H_2 and 1 for o-H_2. Only the

DOI: 10.1021/acs.jpca.7b09762
J. Phys. Chem. A 2018, 122, 1511−1520

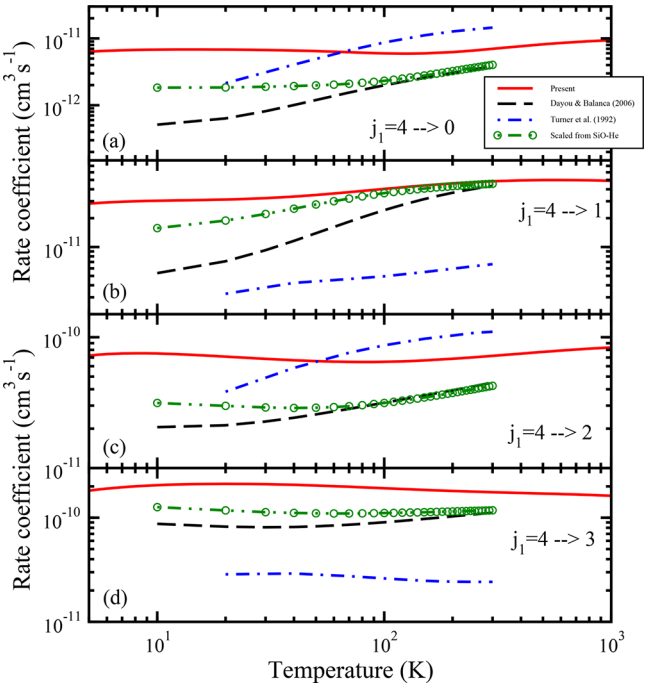

Figure 8. Comparison of current state-to-state rotational quenching rate coefficients with previous approximate results from refs 16 and 22 and obtained from reduced mass scaling of SiO. Rotational transitions of SiO are from $j_1 = 4$ to $j_1' = 0$, 1, 2, and 3, and the collider is p-H_2.

rotational transitions of H_2 are considered, and the vibration of H_2 is fixed in the ground state $v_2 = v_2' = 0$.

For the purpose of illustration, Figure 9 presents the state-to-state and total cross sections for quenching from initial CMS

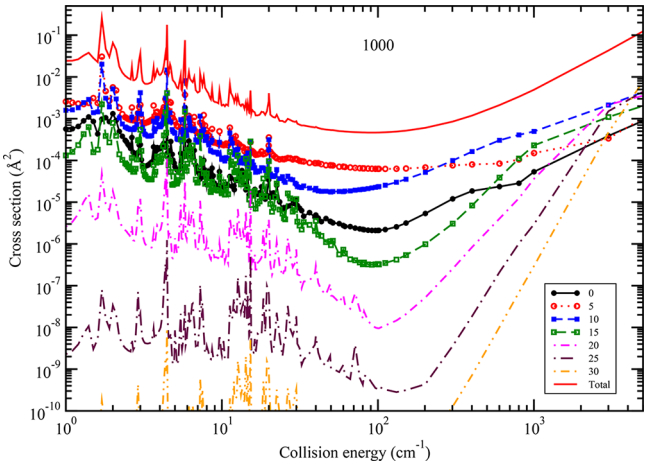

Figure 9. State-to-state and total vibrational quenching cross section for SiO in collisions with p-H_2 with H_2 elasticity ($j_2 = 0 \rightarrow 0$). The initial state is (1000), and final states are $v_1' = 0$, $j_1' = 0$, 5, 10, ..., 30.

(1000) into different final SiO rotational levels in $v_1' = 0$, where we show only $j_1' = 0$, 5, ..., 30 and $j_2 = 0 \rightarrow j_2' = 0$. It can be seen that for the p-H_2 collider the cross sections present a large number of resonances at energies between 1.0 and 200 cm^{-1}, with the resonances extending to a larger collision energy with increasing j_1'. In general, when the collision energies exceed the van der Waals well depth, the state-to-state and total quenching cross sections increase with increasing collision energy. As shown in Figure 9, for the case of p-H_2, the cross section to $j_1' =$ 5 dominates at energies below ~200 cm^{-1}, and then the cross section to $j_1' = 10$ becomes the largest collision energy above 200 cm^{-1}. At $E_c = 5000$ cm^{-1}, the cross section to $j_1' = 0$ is the smallest, while the cross section to $j_1' = 30$ becomes the largest. Cross sections for $j_1' = 20$, 25, and 30 are several orders of magnitude smaller than the other transitions shown in Figure 9 for energies below 500 cm^{-1}. The cross sections for o-H_2 show a similar behavior (see SI).

To show the effect of vibrational excitation on pure rotational cross sections, in Figure 10 we compare cross sections in $v_1 = 0$ and $v_1 = 1$ states. The rotational excitations are from $j_1 = 0$ to $j_1' = 1$, 2, 3, and 4. It can be seen that the pure rotational cross sections are nearly identical for $v_1 = 0$ and 1, except that cross sections for $v_1 = 0$ show strong resonances at low energy. In other words, vibrational excitation has little effect on pure rotational transitions, which might be expected due to the harmonic behavior of the monomer SiO potential.

The vibrational quenching cross sections from initial states (1100) and (1101) are also calculated, in which the excited $j_1 = 1$ levels are considered. Figure 11(a) illustrates the energy dependence of the total $v_1 = 1 \rightarrow v_1' = 0$ quenching cross section with p-H_2 from CMSs (1000) and (1100) for H_2 elastic ($j_2 = 0 \rightarrow j_2' = 0$) and inelastic ($j_2 = 0 \rightarrow j_2' = 2$) transitions. The total quenching cross sections from (1000) and (1100) show some differences for energies less than 40 cm^{-1}, in particular due to different resonance behavior. However, the total quenching cross sections are nearly identical for energies above 40 cm^{-1}, which is likely due to the small energy difference between $j_1 = 0$ and $j_1 = 1$. The cross section corresponding to the inelastic H_2 transition $j_2 = 0 \rightarrow 2$ is about 1 order of magnitude smaller than that for the elastic H_2 transition for energies below 100 cm^{-1}. From Figure 11(b) it can be observed that for the collision with o-H_2 the total vibrational quenching cross sections from initial CMSs (1001) and (1101) show similar behavior. The cross section with an elastic H_2 transition dominates, while the cross sections for $j_2 = 1 \rightarrow 3$ are about two times smaller than the H_2 rotation preserving ($j_2 = 1 \rightarrow 1$) transition. Furthermore, the difference becomes larger with increasing energy; therefore, the cross section for the $j_2 = 1 \rightarrow 3$ transition can be neglected at high collision energies.

The state-to-state and total vibrational quenching rate coefficients are obtained by thermally averaging corresponding cross sections over a Maxwellian distribution of kinetic energy. There are no published theoretical or experimental rate coefficients available.

As an illustration, the total rate coefficients for vibrational quenching from (1000) to $v_1' = 0$ in collisions with p-H_2 ($j_2' = 0$ and 2) and from (1001) to $v_1' = 0$ with o-H_2 ($j_2' = 1$ and 3) are displayed in Figure 12. It can be seen that the total quenching rate coefficients of SiO with H_2 show trends similar to that presented for the total quenching cross sections in Figure 11. Figure 12(a) shows that for SiO with p-H_2, the total vibrational quenching rate coefficients for $\Delta j_2 = 0$ are nearly an order of magnitude larger than the results for $\Delta j_2 = 2$, and between 5 and ~100 K the rate coefficients generally decrease weakly with increasing temperature. For temperatures above ~100 K, the rate coefficients generally increase with increasing temperature. As shown in Figure 12(b), the trends for o-H_2 are very similar to those noted for p-H_2 collisions. The total vibrational quenching rate coefficients for $\Delta j_2 = 0$ are nearly three times larger than the results for $\Delta j_2 = 2$.

DOI: 10.1021/acs.jpca.7b09762
J. Phys. Chem. A 2018, 122, 1511−1520

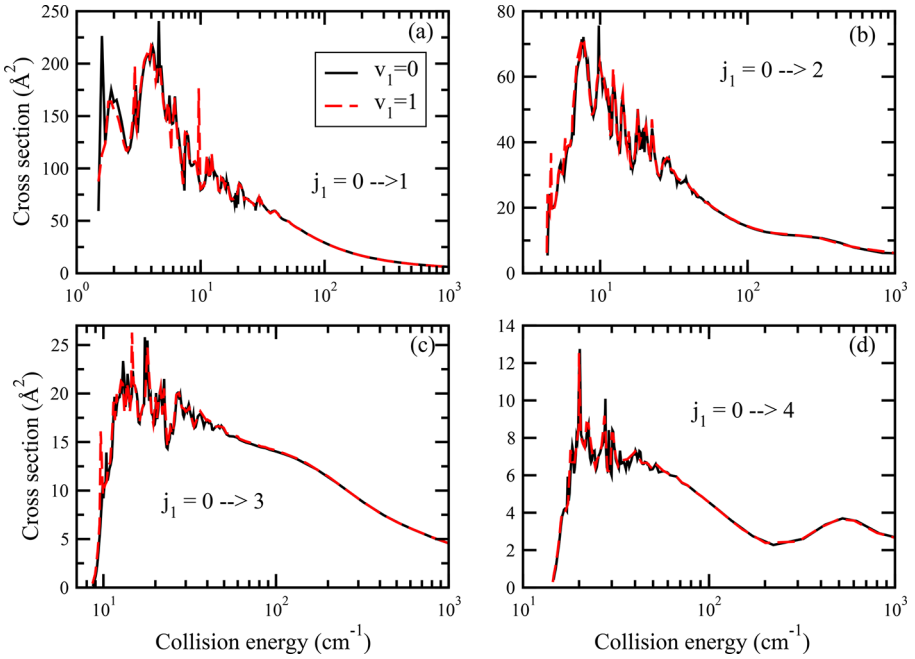

Figure 10. Rotational excitation cross section from $j_1 = 0$ to $j_1' = 1$, 2, 3, and 4 of SiO in collisions with p-H_2. For each transition, the comparison is made between $v_1 = 0$ and $v_1 = 1$.

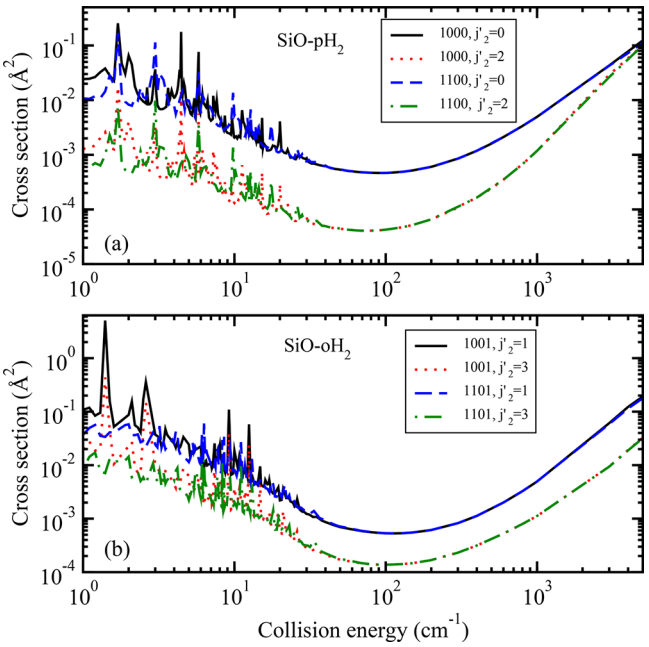

Figure 11. Total vibrational quenching cross sections for SiO in collisions with H_2. (a) Initial states (1000) and (1100), with final $j_2' = 0$ and 2, and (b) initial states (1001) and (1101), with $j_2' = 1$ and 3.

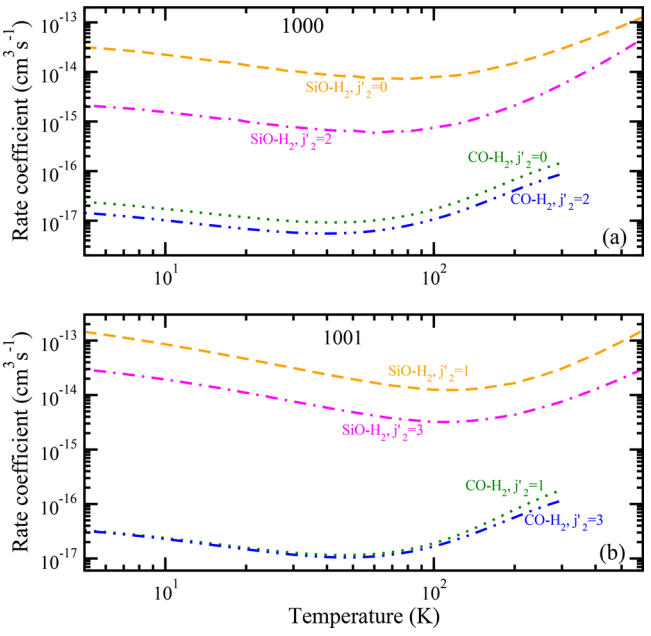

Figure 12. Total rate coefficients for the vibrational quenching of SiO compared to the same transitions for CO from ref 8: (a) from (1000) to $v_1' = 0 + p$-H_2 ($v_2' = 0$, $j_2' = 0$, 2) and (b) from (1001) to $v_1' = 0 + o$-H_2 ($v_2' = 0$, $j_2' = 1$, 3).

In Figure 12 we also compare to results for CO-H_2[8], where it is shown that for the same transitions, CO-H_2 rate coefficients are typically ∼2−3 orders of magnitude smaller than those of SiO-H_2. The large magnitudes of SiO-H_2 rate coefficients are likely related to the fact that the SiO-H_2 PES is more anisotropic. Further, the overall magnitude of the cross sections increases with increasing global well depth: 93.1 (CO-H_2) and 279.5 cm^{-1} (SiO-H_2). The vast difference between the CO and SiO rate coefficients suggests that scaling arguments based on chemical similarities (see ref 46) should be used with caution.

■ ASTROPHYSICAL APPLICATIONS

Emission from interstellar molecular species are used to probe the physical and chemical conditions of the ISM. In particular, observations of rotational and vibrational transitions can provide information on elemental abundances, gas temperature, radiation field, and other local parameters. Since molecular hydrogen is the most abundant species in most cool astrophysical environments, it is usually the dominant collider for molecular emission. While SiO is one of the dominant

DOI: 10.1021/acs.jpca.7b09762
J. Phys. Chem. A 2018, 122, 1511−1520

silicon-containing molecules, elemental silicon is highly depleted onto dust grains in most environments. Nevertheless, SiO emission, including maser lines, have been observed. SiO was first detected by observing the $j_1 = 3-2$ transition near 130.2 GHz with the 11 m Kitt Peak telescope toward Sgr B2(OH).[13] de Vicente and co-workers[47] presented observational results of ^{28}SiO $v_1 = 0$, $j_1 = 1-0$ line emission from 28 evolved stars. Wang and co-workers[48] detected SiO $j_1 = 2-1$ ($v_1 = 3$) mega-maser at 85.038 GHz near the center of the Seyfert 2 galaxy NGC 1068 with the IRAM 30 m telescope. Using the Mopra Telescope of the Australia Telescope National Facility, Indermuehle and McIntosh[49] measured SiO spectra from the $v_1 = 1, j_1 = 1-0$ and the $v_1 = 1, j_1 = 2-1$ transitions. Desmurs and co-workers[50] reported observations of the $v_1 = 1$, $v_1 = 2$, and $v_1 = 3$, $j_1 = 1-0$ maser transitions of SiO in several asymptotic giant branch (AGB) stars using very long baseline interferometry. Two new SiO maser sources, in the high-mass star-forming regions G19.61 − 0.23 and G75.78 + 0.34, were detected by Cho and co-workers,[51] though SiO masers are rare in star-forming regions.

Since silicon is depleted onto grains, it is not detected in protoplanetary disks, though CO is. It is proposed,[52] however, that in the outflows of young stellar objects (YSOs) the grains are disrupted, allowing for the formation of SiO. Observations of SiO may therefore be used to distinguish between the outflow and disk of an YSO. In particular, SiO vibrational emission may trace the wide-angle wind outflow.

However, modeling such spectra requires collisional rate coefficients due to collision by the most abundant species H_2, H, and He. Since it is difficult to measure collisional rate coefficients, astrophysical modeling mainly relies on theoretical results. In previous studies discussed above, approximate SiO-p-H_2 rate coefficients, which were obtained using an SiO-He PES, were adopted, which will lead to significant modeling uncertainty. The current collisional rate coefficients, therefore, will be critical in advancing astrophysical modeling of SiO observations.

SUMMARY

Full-dimensional quantum close-coupling calculations of rotational and vibrational quenching of SiO in collision with p-H_2 ($j_1 = 0$) and o-H_2 ($j_1 = 1$) have been performed for the first time. The considered initial rotational states of SiO are $j_1 = 1-5$ in $v_1 = 0$ and $j_1 = 0$ and 1 in $v_1 = 1$ for collisions with p-H_2 ($j_2 = 0, 2$) and o-H_2 ($j_2 = 1, 3$). The scattering calculations were carried out on a 6D SiO-H_2 interaction potential surface computed using high-level ab initio theory and fitted with an invariant polynomial approach. Pure rotational quenching rate coefficients of SiO in collision with p-H_2 were compared with previous approximate results obtained using SiO-He potentials or mass scaling methods. State-to-state and total quenching cross sections from the SiO vibrational state $v_1 = 1$ show resonance structures at intermediate energies for both p-H_2 and o-H_2. The state-to-state rate coefficients for both rotational and vibrational quenching were computed for temperatures ranging from 5 to 1000 K. Calculations of quenching from higher excited rotational and vibrational states of SiO are in progress. The current calculations together with large-scale coupled-states (CS) approximation[12] results will be essential in the construction of a database of SiO rotational and vibrational quenching rate coefficients urgently needed for astrophysical modeling.[18−20,53]

ASSOCIATED CONTENT

Supporting Information

The Supporting Information is available free of charge on the ACS Publications website at DOI: 10.1021/acs.jpca.7b09762.

A Fortran subroutine for generating the 6D VSiOH2 PES (ZIP)

Anisotropy of the VSiOH2 PES for R = 6.0, 6.5, 7.0, and 8.0 a_0 (Figure S1); rotational state-to-state de-excitation cross sections for SiO with p-H_2, j_1 = 1, 3, and 5 (Figure S2); rotational state-to-state de-excitation cross sections for SiO with p-H_2, j_1 = 2 and 4 (Figure S3); rotational state-to-state de-excitation cross sections for SiO with o-H_2, j_1 = 2 and 4 (Figure S4); rotational state-to-state de-excitation rate coefficients for SiO with o-H_2, j_1 = 1, 3, and 5 (Figure S5); state-to-state and total vibrational quenching cross section for SiO in collisions with o-H_2 (Figure S6); comparison of the distributions of final rotational levels in $v_1' = 0$ quenching from CMSs (1000) and (1001) at E_c = 1.0, 10.0, and 100.0 cm^{-1} (Figure S7); state-to-state and total vibrational quenching rate coefficients for SiO in collisions with o-H_2 (Figure S8) (PDF)

AUTHOR INFORMATION

Corresponding Author

*E-mail: yang@physast.uga.edu.

ORCID

Benhui Yang: 0000-0002-9667-715X

J. M. Bowman: 0000-0001-9692-2672

Notes

The authors declare no competing financial interest.

ACKNOWLEDGMENTS

Work at the University of Georgia (UGA) and Emory was supported by NASA (NNX16AF09G), at the University of Nevada, Las Vegas (UNLV) by the NSF (PHY-1505557), and at Penn State by the NSF (PHY-1503615). B.M.M. acknowledges the University of Georgia for travel funding and Queen's University Belfast for the award of a research fellowship. This study was supported in part by resources and technical expertise from the UGA Georgia Advanced Computing Resource Center (GACRC) and the UNLV National Supercomputing Institute & Dedicated Research Network. We thank Shan-Ho Tsai (GACRC), Jeff Deroshia (UGA Department of Physics and Astronomy), and Ron Young (UNLV) for computational assistance. Portions of the potential surface calculations were performed at the National Energy Research Scientific Computing Center (NERSC) in Berkeley, CA, USA, and at the High Performance Computing Center Stuttgart (HLRS) of the University of Stuttgart, Stuttgart, Germany, where grants of time are gratefully acknowledged.

ADDITIONAL NOTE

[a]Figures for other initial states, as well as for o-H_2 colliders, can be found in the Supporting Information.

REFERENCES

(1) Flower, D. *Molecular Collisions in the Interstellar Medium*, 2nd ed.; Cambridge University Press: Cambridge, U.K., 2011.

DOI: 10.1021/acs.jpca.7b09762
J. Phys. Chem. A 2018, 122, 1511−1520

(2) Takayanagi, K. The production of rotational and vibrational transitions in encounters between molecules. *Adv. At. Mol. Phys.* **1965**, *1*, 149−194.
(3) Pogrebnya, S. K.; Clary, D. C. A full-dimensional quantum dynamical study of vibrational relaxation in H_2+H_2. *Chem. Phys. Lett.* **2002**, *363*, 523−528.
(4) Krems, R. V. *TwoBC − Quantum Scattering Program*; University of British Columbia: Vancouver, Canada, 2006.
(5) Quéméner, G.; Balakrishnan, N. Quantum calculations of H_2-H_2 collisions: From ultracold to thermal energies. *J. Chem. Phys.* **2009**, *130*, 114303.
(6) dos Santos, S. F.; Balakrishnan, N.; Lepp, S.; Quéméner, G.; Forrey, R. C.; Hinde, R. J.; Stancil, P. C. Quantum dynamics of rovibrational transitions in H_2-H_2 collisions: Internal energy rotational angular momentum conservation effects. *J. Chem. Phys.* **2011**, *134*, 214303.
(7) dos Santos, S. F.; Balakrishnan, N.; Forrey, R. C.; Stancil, P. C. Vibration-vibration and vibration-translation energy transfer in H_2-H_2 collisions: A critical test of experiment with full-dimensional quantum dynamics. *J. Chem. Phys.* **2013**, *138*, 104302.
(8) Yang, B. H.; Zhang, P.; Wang, X.; Stancil, P. C.; Bowman, J. M.; Balakrishnan, N.; Forrey, R. C. Quantum dynamics of CO-H_2 in full dimensionality. *Nat. Commun.* **2015**, *6*, 6629.
(9) Yang, B. H.; Balakrishnan, N.; Zhang, P.; Wang, X.; Bowman, J. M.; Forrey, R. C.; Stancil, P. C. Full-dimensional quantum dynamics of CO in collision with H_2. *J. Chem. Phys.* **2016**, *145*, 034308.
(10) Yang, B. H.; Wang, X.; Stancil, P. C.; Bowman, J. M.; Balakrishnan, N.; Forrey, R. C. Full-dimensional quantum dynamics of rovibrationally inelastic scattering between CN and H_2. *J. Chem. Phys.* **2016**, *145*, 224307.
(11) Bohr, A.; Paolini, S.; Forrey, R. C.; Balakrishnan, N.; Stancil, P. C. A full-dimensional quantum dynamical study of H_2+H_2 collisions: Coupled-states versus close-coupling formulation. *J. Chem. Phys.* **2014**, *140*, 064308.
(12) Forrey, R. C.; Yang, B. H.; Stancil, P. C.; Balakrishnan, N. Mutual vibrational quenching in CO + H_2 collisions. *Chem. Phys.* **2015**, *462*, 71−78.
(13) Wilson, R. W.; Penzias, A. A.; Jefferts, K. B.; Kutner, M.; Thaddeus, P. Discovery of Interstellar Silicon Monoxide. *Astrophys. J.* **1971**, *167*, L97.
(14) Fonfría, J. P.; Fernández-López, M.; Agúndez, M.; Sánchez-Contreras, C.; Curiel, S.; Cernicharo, J. The complex dust formation zone of the AGB star IRC+10216 probed with CARMA 0.25 arcsec angular resolution molecular observations. *Mon. Not. R. Astron. Soc.* **2014**, *445*, 3289−3308.
(15) Tercero, B.; Vincent, L.; Cernicharo, J.; Viti, S.; Marcelino, N. A line-confusion limited millimeter survey of Orion KL. II. Silicon-bearing species. *Astron. Astrophys.* **2011**, *528*, A26.
(16) Dayou, F.; Balança, C. Rotational excitation of SiO by collisions with helium. *Astron. Astrophys.* **2006**, *459*, 297−305.
(17) Velilla Prieto, L.; Sánchez Contreras, C.; Cernicharo, J.; Agúndez, M.; Quintana-Lacaci, G.; Bujarrabal, V.; Alcolea, J.; Balança, C.; Herpin, F.; Menten, K. M.; Wyrowski, F. The millimeter IRAM-30m line survey toward IK Tauri. *Astron. Astrophys.* **2017**, *597*, A25.
(18) Agúndez, M.; Fonfría, J. P.; Cernicharo, J.; Kahane, C.; Daniel, F.; Guélin, M. Molecular abundances in the inner layers of IRC + 10216. *Astron. Astrophys.* **2012**, *543*, A48.
(19) Justtanont, K.; Khouri, T.; Maercker, M.; Alcolea, J.; Decin, L.; Olofsson, H.; Schöier, F. L.; Bujarrabal, V.; Marston, A. P.; Teyssier, D.; et al. Herschel/HIFI observations of O-rich AGB stars: molecular inventory. *Astron. Astrophys.* **2012**, *537*, A144.
(20) Matsuura, M.; Yates, J. A.; Barlow, M. J.; Swinyard, B. M.; Royer, P.; Cernicharo, J.; Decin, L.; Wesson, R.; Polehampton, E. T.; Blommaert, J. A. D. L.; et al. Herschel SPIRE and PACS observations of the red supergiant VY CMa: analysis of the molecular line spectra. *Mon. Not. R. Astron. Soc.* **2013**, *437*, 532−546.
(21) Balança, C.; Dayou, F. Ro-vibrational excitation of SiO by collision with helium at high temperature. *Mon. Not. R. Astron. Soc.* **2017**, *469*, 1673−1681.
(22) Turner, B. E.; Chan, K.-W.; Green, S.; Lubowich, D. A. Tests of shock chemistry in IC 443G. *Astrophys. J.* **1992**, *399*, 114−133.
(23) Bieniek, R. J.; Green, S. Electron-gas He-SiO potential hypersurface for vibrational- rotational excitations through collisions. *Chem. Phys. Lett.* **1981**, *84*, 380−384.
(24) Braams, B. J.; Bowman, J. M. Permutationally invariant potential energy surfaces in high dimensionality. *Int. Rev. Phys. Chem.* **2009**, *28*, 577−606.
(25) Werner, H.-J.; Knowles, P. J.; Knizia, G.; Manby, F. R.; Schütz, M. Molpro: a general purpose quantum chemistry program package. *WIREs Comput. Mol. Sci.* **2012**, *2*, 242−253.
(26) Werner, H.-J.; Knowles, P. J.; Knizia, G.; Manby, F. R.; Schütz, M.; Celani, P.; Györffy, W.; Kats, D.; Korona, T.; Lindh, R.; et al. *MOLPRO, version 2010.1, a package of ab initio programs*; http://www.molpro.net.
(27) Adler, T. B.; Knizia, G.; Werner, H.-J. A simple and efficient CCSD(T)-F12 approximation. *J. Chem. Phys.* **2007**, *127*, 221106.
(28) Werner, H.-J.; Adler, T. B.; Manby, F. R. General orbital invariant MP2-F12 theory. *J. Chem. Phys.* **2007**, *126*, 164102.
(29) Kendall, R. A.; Dunning, T. H., Jr.; Harrison, R. J. Electron affinities of the first-row atoms revisited. Systematic basis sets and wave functions. *J. Chem. Phys.* **1992**, *96*, 6796−6806.
(30) Peterson, K. A.; Dunning, T. H., Jr. Accurate correlation consistent basis sets for molecular core-valence correlation effects. The second row atoms Al-Ar, and the first row atoms B-Ne revisited,. *J. Chem. Phys.* **2002**, *117*, 10548−10560.
(31) Weigend, F.; Köhn, A.; Hättig, C. Efficient use of the correlation consistent basis sets in resolution of the identity MP2 calculations. *J. Chem. Phys.* **2002**, *116*, 3175−3183.
(32) Hättig, C. Optimization of auxiliary basis sets for RI-MP2 and RI-CC2 calculations: Core-valence and quintuple-ζ basis sets for H to Ar and QZVPP basis sets for Li to Kr. *Phys. Chem. Chem. Phys.* **2005**, *7*, 59−66.
(33) EMSL basis set exchange, https://bse.pnl.gov/bse/portal.
(34) Boys, S. F.; Bernardi, F. The calculation of small molecular interactions by differences of separate total energies - some procedures with reduced errors. *Mol. Phys.* **1970**, *19*, 553−566.
(35) Feller, D.; Peterson, K. A.; Hill, J. G. Calibration study of the CCSD(T)-F12a/b methods for C_2 and small hydrocarbons. *J. Chem. Phys.* **2010**, *133*, 184102.
(36) Bowman, J. M.; Braams, B. J.; Carter, S.; Chen, C.; Czakó, G.; Fu, B.; Huang, X.; Kamarchik, E.; Sharma, A. R.; Shepler, B. C.; et al. Ab-initio-based potential energy surfaces for complex molecules and molecular complexes. *J. Phys. Chem. Lett.* **2010**, *1*, 1866−1874.
(37) Xie, Z.; Bowman, J. M. Permutationally invariant polynomial basis for molecular energy surface fitting via monomial symmetrization. *J. Chem. Theory Comput.* **2010**, *6*, 26−34.
(38) Green, S. Rotational excitation in H_2-H_2 collisions - close-coupling calculations. *J. Chem. Phys.* **1975**, *62*, 2271−2277.
(39) Alexander, M. H.; DePristo, A. E. Symmetry considerations in quantum treatment of collisions between two diatomic-molecules. *J. Chem. Phys.* **1977**, *66*, 2166−2172.
(40) Zarur, G.; Rabitz, H. Effective potential formulation of molecule-molecule collisions with application to H_2-H_2. *J. Chem. Phys.* **1974**, *60*, 2057−2078.
(41) Johnson, B. R. Multichannel log-derivative method for scattering calculations. *J. Comput. Phys.* **1973**, *13*, 445−449.
(42) Barton, E. J.; Yurchenko, S. N.; Tennyson, J. ExoMol line lists - II. The ro-vibrational spectrum of SiO. *Mon. Not. R. Astron. Soc.* **2013**, *434*, 1469−1475.
(43) Schwenke, D. W. Calculations of rate constants for the three-body recombination of H_2 in the presence of H_2. *J. Chem. Phys.* **1988**, *89*, 2076−2091.
(44) Schöier, F. L.; van der Tak, F. F. S.; van Dishoeck, E. F.; Black, J. H. An atomic and molecular database for analysis of submillimetre line observations. *Astron. Astrophys.* **2005**, *432*, 369−379.
(45) Walker, K. M.; Yang, B. H.; Stancil, P. C.; Balakrishnan, N.; Forrey, R. C. On the Validity of Collider-mass Scaling for Molecular Rotational Excitation. *Astrophys. J.* **2014**, *790*, 96.

DOI: 10.1021/acs.jpca.7b09762
J. Phys. Chem. A 2018, 122, 1511−1520

(46) Van der Tak, F. In *The Molecular Universe, Proc. IAU Symposium 280*; Cernicharo, J., Bachiller, R., Eds.; Cambridge University Press: Cambridge, U.K., 2011.
(47) de Vicente, P.; Bujarrabal, V.; Díaz-Pulido, A.; Albo, C.; Alcolea, J.; Barcia, A.; Barbas, L.; Bolaño, R.; Colomer, F.; Diez, M. C.; et al. ^{28}SiO $v = 0$ $J = 1-0$ emission from evolved stars. *Astron. Astrophys.* **2016**, *589*, A74.
(48) Wang, J.; Zhang, J.; Gao, Y.; Zhang, Z.-Y.; Li, D.; Fang, M.; Shi, Y. SiO and CH_3OH mega-masers in NGC 1068. *Nat. Commun.* **2014**, *5*, 5449.
(49) Indermuehle, B. T.; McIntosh, G. C. A phase-dependent comparison of the velocity parameters of SiO $v = 1$, $J = 1-0$ and $J = 2-1$ maser emission in long-period variables. *Mon. Not. R. Astron. Soc.* **2014**, *441*, 3226−3230.
(50) Desmurs, J.-F.; Bujarrabal, V.; Lindqvist, M.; Alcolea, J.; Soria-Ruiz, R.; Bergman, P. SiO masers from AGB stars in the vibrationally excited $v = 1$, $v = 2$, and $v = 3$ states. *Astron. Astrophys.* **2014**, *565*, A127.
(51) Cho, S.-H.; Yun, Y.; Kim, J.; Liu, T.; Kim, K.-T.; Choi, M. Two New SiO Maser Sources in High-Mass Star-forming Regions. *Astrophys. J.* **2016**, *826*, 157.
(52) Tan, J. C.; Beltrán, M. T.; Caselli, P.; Fontani, F.; Fuente, A.; Krumholz, M. R.; McKee, C. F.; Stolte, A. Massive Star Formation. In *Protostars and Planets VI*; Buether, H., Klessen, R. S., Dullemond, C. P., Henning, T., Eds.; University of Arizona Press: Tucson, AZ, 2014; pp 149−172.
(53) Zhang, Z.; Stancil, P. C.; Cumbee, R. C.; Ferland, G. J. Ro-vibrational analysis of SiO. *Mon. Not. R. Astron. Soc.*, 2017, to be submitted.

DOI: 10.1021/acs.jpca.7b09762
J. Phys. Chem. A 2018, 122, 1511−1520